GEOPHYSICAL RESEARCH LETTERS, VOL. 40, 5548–5552, doi:10.1002/2013GL057454, 2013

Disentangling Mie and attenuation effects in rain using a K_a-W dual-wavelength Doppler spectral ratio technique

Frédéric Tridon,[1] Alessandro Battaglia,[1] and Pavlos Kollias[2]

Received 24 July 2013; revised 1 October 2013; accepted 9 October 2013; published 24 October 2013.

[1] A novel technique that enables to disentangle Mie and attenuation effects in coincident, beam-matched K_a- and W-band radar observations is presented here. The ratio of the measured radar Doppler spectra at the two frequencies is estimated, and the Doppler velocity regime that corresponds to Rayleigh scatterers is determined. The range variation of the Rayleigh regime "plateau" is directly linked to the differential attenuation between the two wavelengths and does represent the attenuation component of the dual-wavelength ratio. The retrieval technique is applied to a light stratiform rain event and provides plausible results. The proposed Doppler spectral ratio methodology has potential for applications in precipitating snow, liquid and ice clouds and can be extended to other wavelength pairs. **Citation:** Tridon, F., A. Battaglia, and P. Kollias (2013), Disentangling Mie and attenuation effects in rain using a K_a-W dual-wavelength Doppler spectral ratio technique, *Geophys. Res. Lett.*, *40*, 5548–5552, doi:10.1002/2013GL057454.

1. Introduction

[2] Multiwavelength radar techniques are widely used for various cloud and rain retrievals. They rely on the wavelength dependence of scattering and absorption properties at millimeter wavelength [*Kollias et al.*, 2007]. Cloud and rain are good absorbers, and the radar attenuation typically increases with frequency. This characteristic has been exploited by dual-wavelength differential attenuation methods like the estimation of the cloud, drizzle, or light rain liquid water contents [*Hogan et al.*, 2005; *Ellis and Vivekanandan*, 2011]. However, these techniques are not always applicable since, if drops diameters are comparable to at least one of the radars wavelength, the measured differential reflectivity includes a "Mie effect," practically indistinguishable from differential attenuation effects.

[3] Conversely, Mie effects have been used for sizing and for hydrometeor classification in snow and ice clouds [*Matrosov*, 1998; *Wang et al.*, 2005; *Liao and Meneghini*, 2011]. Again, a limitation resides in a potential non-negligible differential attenuation (e.g., due to gases, supercooled liquid layers, or the ice itself) indistinguishable from the Mie effects.

[4] In rain, dual-wavelength measurements at K_a and W band are subject to both attenuation and Mie effects. The use of a third wavelength could offer a Rayleigh scattering reference, but it is challenging to match the triple-wavelength observations in time and space. This paper presents a novel technique able to disentangle these two quantities from a K_a-W-band pair Doppler spectral measurements. After the presentation of the principle of dual-wavelength measurements, the Doppler spectral ratio technique is demonstrated via simulated spectra and applied to a stratiform light rain event measured at the Department Of Energy (DOE) Atmospheric Research Measurement (ARM) Program Southern Great Plains (SGP) site.

2. Dual-Wavelength Radar Measurements

[5] The effective reflectivity factor $Z_{e,\lambda}$ at range r and at a given wavelength λ is defined by

$$Z_{e,\lambda}(r) = \frac{\lambda^4}{\pi^5 |K_W|^2} \eta(r) \tag{1}$$

where η is the radar reflectivity and $|K_W|^2 = 0.93$ is related to the complex refractive index of water at centimeter wavelengths. If the Rayleigh conditions are satisfied, that is, when scattering particles are much smaller than the radar wavelength, η is proportional to λ^{-4}, and $Z_{e,\lambda}$ does not depend on wavelength; otherwise it differs from its Rayleigh counterpart by the so-called Mie effects, which depend on the wavelength and the type and size of hydrometeors present in the scattering volume.

[6] The measured reflectivity factor can be expanded in logarithmic units as follows:

$$Z_{m,\lambda}(r) = Z_{e,\lambda}(r) - 2\int_0^r (\alpha_\lambda(s))\mathrm{d}s \tag{2}$$

where α_λ, is the one-way specific attenuation at a given wavelength and accounts for attenuation by gases, hydrometeors, and wet radome.

[7] Dual-wavelength techniques generally use the dual-wavelength ratio (DWR) defined as the ratio of reflectivity factor measurements from two collocated radars operating at different wavelengths λ_1 and λ_2 ($\lambda_1 > \lambda_2$):

$$\begin{aligned}\mathrm{DWR}(r) &\equiv Z_{m,\lambda_1}(r) - Z_{m,\lambda_2}(r) \\ &= \underbrace{Z_{e,\lambda_1}(r) - Z_{e,\lambda_2}(r)}_{\text{Mie effect}} + \underbrace{2\int_0^r (\alpha_{\lambda_2}(s) - \alpha_{\lambda_1}(s))\,\mathrm{d}s}_{\text{Attenuation effect}}.\end{aligned} \tag{3}$$

Since "Mie and differential attenuation effects" are indistinguishable within the total DWR, so far dual-wavelength techniques have been developed for conditions where one effect is negligible. For instance, the Mie-dominated DWR

[1]Earth Observation Sciences, Department of Physics and Astronomy, University of Leicester, Leicester, UK.
[2]Department of Atmospheric and Oceanic Sciences, McGill University, Montreal, Quebec, Canada.

Corresponding author: F. Tridon, Earth Observation Sciences, Department of Physics and Astronomy, University of Leicester, University road, Leicester, LE1 7RH, UK. (f.tridon@leicester.ac.uk)

0094-8276/13/10.1002/2013GL057454

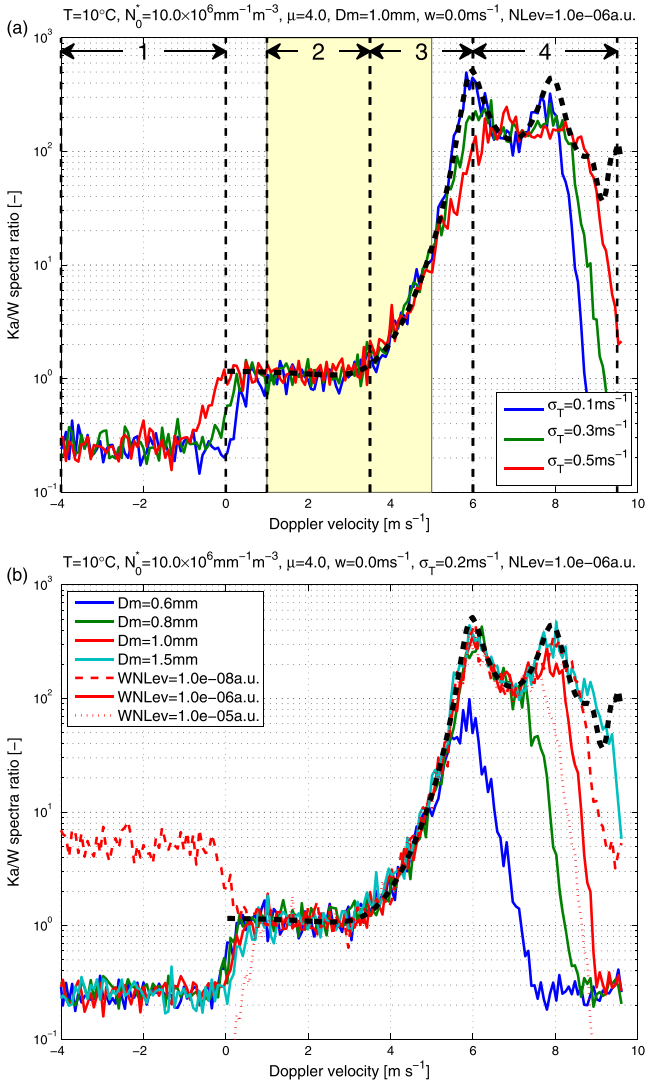

Figure 1. Simulations of the K_a/W spectral ratio for (a) different turbulence intensities, (b) different mean volume diameter of the drop size distribution (continuous lines) and different noise levels in W-band spectra (red lines). Other parameters are taken constant and are described in the title of Figures 1a and 1b.

can be used for sizing particles in ice clouds; conversely, the attenuation-dominated DWR is related to the liquid water content in stratocumulus clouds.

[8] However, for DWR techniques to be effective in general conditions, the separation of these two components is needed. Previous attempts used an additional constraint like the path-integrated attenuation for satellite-borne measurements [*Meneghini et al.*, 2012], or an extra wavelength [*Gaussiat et al.*, 2003]. The technique proposed here uses Doppler spectral measurements but does not need any additional constraint.

3. K_a-W Doppler Spectral Ratio Technique

[9] For ground based Doppler radars, the hydrometeor radar Doppler spectrum $S_{\mathrm{hyd},\lambda}$ is generally produced by a fast Fourier transform of the received signal and is proportional to the particle size distribution (PSD) $N(D)$ and the attenuated backscattering cross section $\sigma_{\lambda,\mathrm{att}}$, according to

$$S_{\mathrm{hyd},\lambda}(v) = N(D)\sigma_{\lambda,\mathrm{att}}(D)\frac{\mathrm{d}D}{\mathrm{d}v} \tag{4}$$

where $\mathrm{d}D/\mathrm{d}v$ represents the coordinate transformation from the terminal velocity v to the diameter D space. Then, the dual-wavelength Doppler spectral ratio (DSR) is simply proportional to the λ^4-scaled ratio of $\sigma_{\lambda,\mathrm{att}}$ at these wavelengths, which is well predicted by scattering theories. Even if the Rayleigh conditions are not satisfied for the whole PSD, the smallest particles scatter the radar wave in the Rayleigh regime. As a result, the corresponding part of the measured

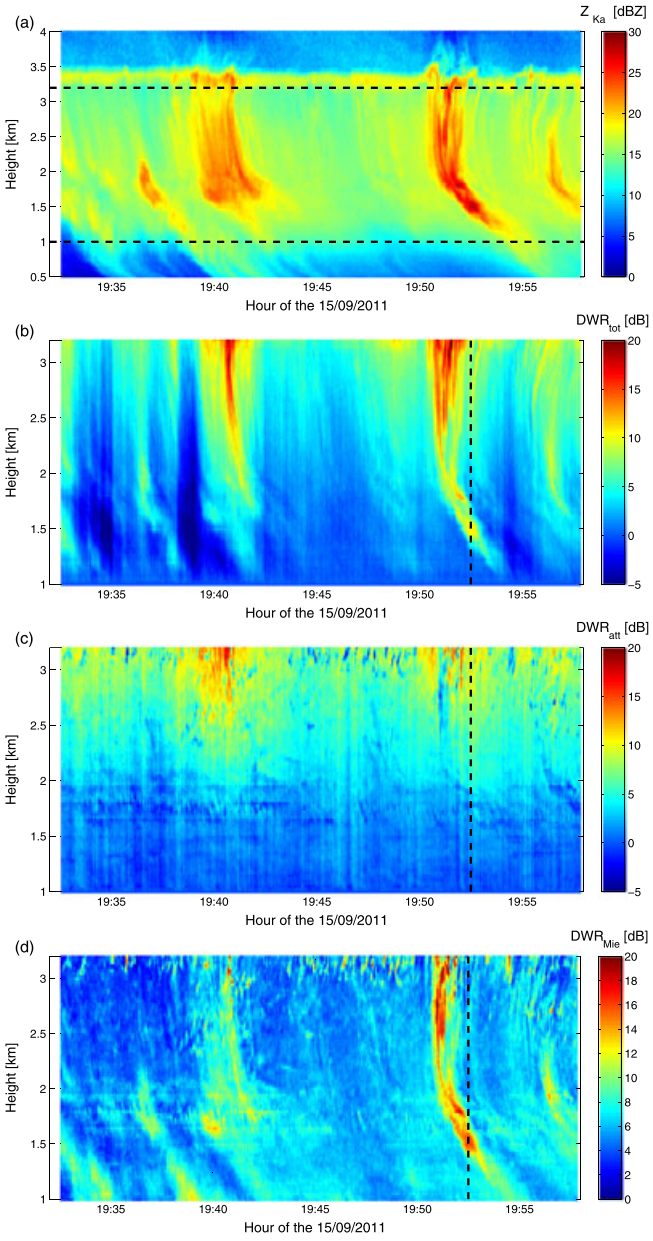

Figure 2. Time-height plots of the reflectivity measured by the (a) KAZR and of the (b) total DWR between KAZR and WSACR on 15 September 2011, between 19:30 and 20:00 UTC. The corresponding (c) two-way rain and gas differential attenuation and (d) Mie components are inferred from the DSR technique.

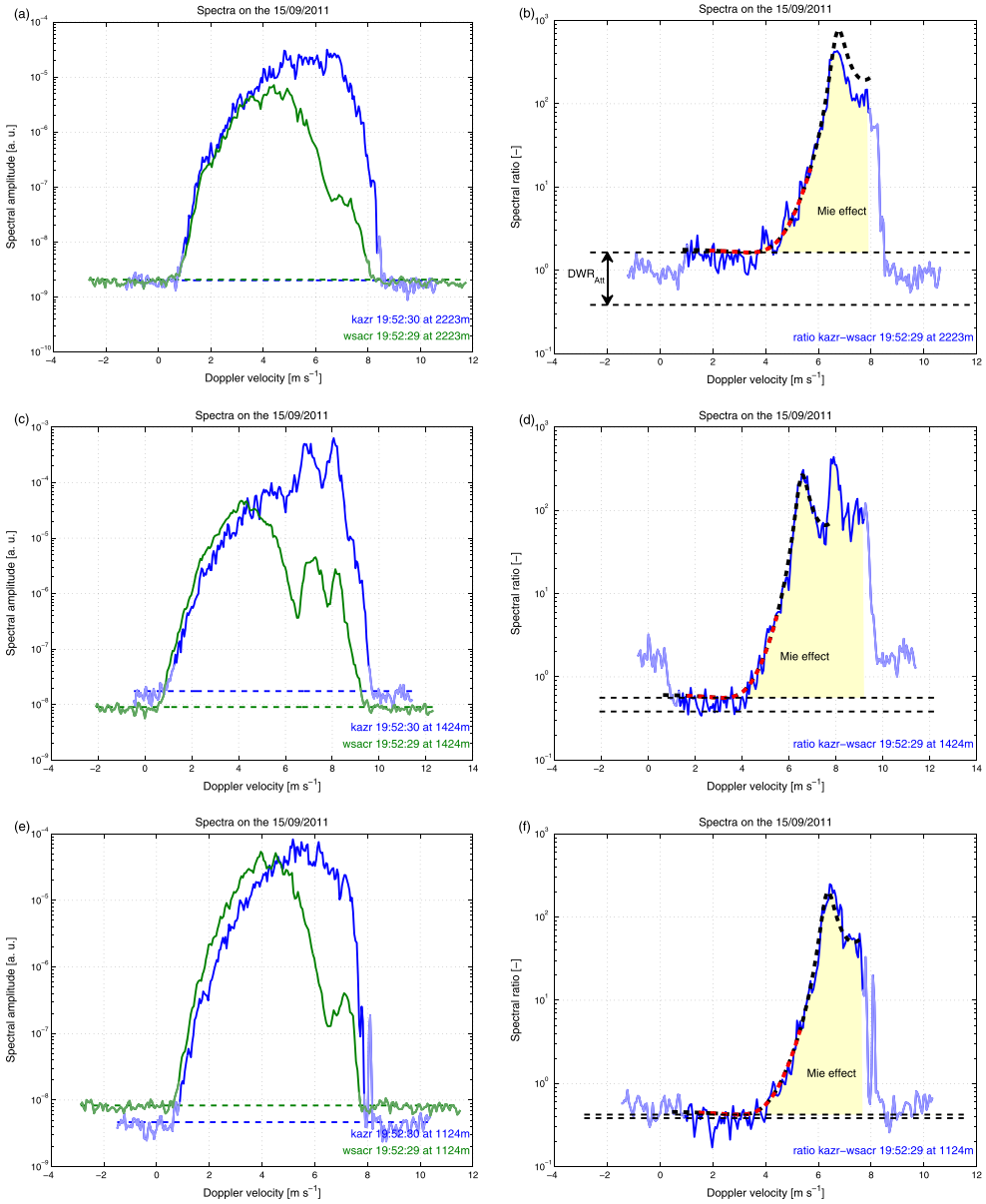

Figure 3. (a,c,e) Dealiased spectra from the KAZR (blue) and the WSACR (green) for different heights and (b,d,f) their corresponding Doppler spectral ratio at 19:52:29 UTC (velocity bins where the SNR of at least one radar is below 5 dB are not considered (light colored parts)). The dashed red line indicate the part of the theoretical DSR which is fitted to the curves, while the extended curve (thick black lines) is plotted for visual consistency check. The fact that the observed peak at 2223 m (Figure 3b) is not as high as the predicted one is probably due to slightly larger turbulence at this level.

Doppler spectra should be identical and their ratio appear as a plateau.

[10] In reality, the measured Doppler spectrum $S_{m,\lambda}$ is affected by the vertical wind w and the turbulence spectrum $T(\sigma_T, v)$ whose spectrum width σ_T depends on antenna beam width $\theta_{3\mathrm{dB}}$, pulse length τ, dwell time t_d and eddy dissipation rate ϵ through [*Doviak and Zrnić*, 1984; *Kollias et al.*, 2011]:

$$S_{m,\lambda}(v+w) = T(\sigma_T(\theta_{3\mathrm{dB}}, \tau, t_d, \epsilon), v) * S_{\mathrm{hyd},\lambda}(v+w). \quad (5)$$

While w simply shifts both spectra, T can alter the DSR shape through its convolution ($*$) with each spectrum.

[11] As a demonstration, simulations of the K_a- over W-band DSR in rain are performed using a three-parameter (normalized intercept parameter N_0^*, mean volume diameter D_m, and shape parameter μ) gamma representation of the PSD, for various conditions of signal to noise ratio (SNR) and turbulence, with T-matrix calculations of the backscattering cross section and a typical relation between the diameter and fall velocity of drops [*Atlas et al.*, 1973]. The stochastic nature of reflectivity measurements is simulated using exponentially distributed samples [*Doviak and Zrnić*, 1984].

[12] Figure 1a shows the λ^4-scaled ratio of K_a/W backscattering cross sections (thick dashed black line) superimposed with DSRs (thin continuous lines) simulated using various turbulence broadening typically expected for the beam geometry of the ARM radars [*Mather and Voyles*, 2013]. Four regions can be identified: (1) a noise region

where both radar signals are within their noise level; (2) a Rayleigh plateau ($D < 0.8$ mm); (3) an upsloping Mie region where the signal is typically increasing by more than two orders of magnitude; and (4) a peak and valley Mie region ($D > 2$ mm) as a result of the W-band backscattering cross-section oscillations [*Kollias et al.*, 2002]. These results show that the DSR shape in the Rayleigh plateau and in the upsloping Mie region (yellow shaded region) is almost immune to the turbulence.

[13] The DSR Mie region appears only if the corresponding drops are sufficiently abundant in the backscattering volume. However, simulations using various values of D_m (Figure 1b) show that drops of 1.5 mm ($v \approx 5$ m s^{-1}) are sufficient to produce a significant upsloping Mie region which expands over more than one order of magnitude. Finally, the transition zone between the noise region and the Rayleigh plateau widens for low K_a- or W-band SNRs (red curves in Figure 1b correspond to different W-band SNRs), however, as long as the right part of the Rayleigh plateau has a good SNR, the DSR major features are not affected.

[14] In conclusion, the Rayleigh plateau and the upsloping region ($v \approx 1-5$ m s^{-1}) constitute a characteristic pattern, which can be fitted to the measured DSR. Its level increases with height according to the differential attenuation between W and K_a and can be used to retrieve the two-way attenuation component DWR_{Att} in the DWR total variation (DWR_{Tot}) between two heights. The Mie component DWR_{Mie} can be determined in an absolute manner, as the difference between the reflectivities computed from the spectra after their respective adjustment in the Rayleigh scattering region, by forcing the Rayleigh plateau level to be equal to unity.

[15] This technique is analogous to the high spectral resolution lidar technique [*Piironen and Eloranta*, 1994], where the Mie (aerosol/hydrometeors) signal is separated from the Rayleigh (molecular) signal using spectral filtering of the data.

4. Observations

[16] As this technique requires highly matched resolution volume, it was applied to measurements from the collocated K_a-band ARM Zenith-pointing Radar (KAZR) and the W-band Scanning ARM Cloud Radar (WSACR), whose beam widths are 0.2° and 0.3°, vertical volume resolutions are 45 m and 52 m, and sampling resolutions are 30 m and 25 m, respectively. While the horizontal mismatch is mitigated by the integration time (2 s for both radars), the matching in range is of particular importance and was done by the selection of the closest gates.

[17] The retrievals were applied on a low turbulence light stratiform rain case with larger reflectivity fall streaks (Figure 2a, reflectivities may be subject to wet radome attenuation) occurred at the ARM SGP Central Facility on 15 September 2011, only between 1 and 3.2 km in order to avoid the melting layer and the very weak SNRs below 1 km (where the wind shear blows the rain away of the line of sight of the radars). As expected, because of rain and gas attenuation, the DWR_{Tot} normalized to the reflectivities at 1 km (Figure 2b) generally increases with height except right above the fall streaks. Important Mie effects due to large drops in the fall streaks may explain these features.

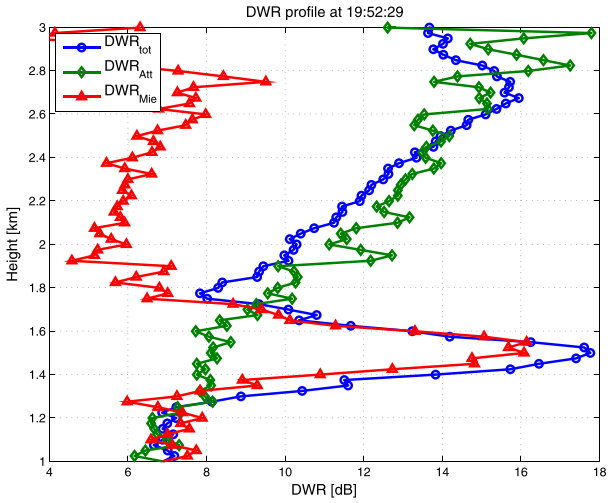

Figure 4. Profiles of the total DWR (blue line with circle marks) between KAZR and WSACR and its Mie (two-way rain and gas differential attenuation) component with a red line and triangle marks (green line with diamond marks) at 19:52:29 UTC.

[18] Figures 3a, 3c, and 3e show the dealiased Doppler spectra measured by the two radars at 19:52:30 below, within and above one of the fall streaks. Because of a dynamic range limitation of around 50 dB, the noise levels can vary with height [*Tridon et al.*, 2013]. However, after the detection [*Hildebrand and Sekhon*, 1974] and rejection of the noise part, the corresponding DSRs can be derived safely. These DSRs (Figures 3b, 3d, and 3f) have the expected features, and the universal part of the theoretical DSR is fitted to determine the level of the Rayleigh plateau. By comparison with its reference value at 1 km height (thin dashed black lines), the plateau level monotonically increases with two-way rain and gas attenuation from the lowest to the highest gates (bottom to top), indicating that the higher DWR in the fall streak (Figure 2b) is indeed due to larger Mie effects (yellow shaded region). The full profile of DWR_{Att} relative to the 1 km height roughly follows DWR_{Tot} (Figure 4), except around 1.5 km because of the larger DWR_{Mie} of the fall streak. This is further confirmed by DWR_{Att} and DWR_{Mie} components for the full case (Figures 2c and 2d). Note that DWR_{Att} is noisy (accuracy of around 1 dB), because of the stochastic nature of spectral measurements, but, as this is a very high resolution product (2 s and 30 m), temporal and vertical averaging can reduce such variability.

5. Conclusion

[19] This paper presents a novel technique to disentangle the Mie and attenuation effects from Ka-W Doppler spectral measurements. The key is to use the DSR in order to remove most of the dependence on the PSD. Simulations show that in rain, this DSR has a quasi-universal shape (a Rayleigh plateau next to an upsloping Mie region); this is confirmed by measurements. The range variation of the Rayleigh plateau level is directly linked to the differential attenuation between the two wavelengths and represents the attenuation component of the DWR, the latter including both hydrometeors and gas attenuation.

[20] The technique is successfully applied on a stratiform light rain event, but it is potentially suitable for drizzling stratocumulus and for higher rain rates, as long as the W-band signal corresponding to drops between roughly 0.5 and 1.5 mm remains well above the noise level. Generalization to G band radars can also pave the way toward applications related to snow (e.g., identification of supercooled liquid layers, validation of nonspherical ice scattering models).

[21] **Acknowledgments.** The authors thank two anonymous reviewers for their helpful comments and greatly acknowledge E. Luke for interesting discussions about radar Doppler spectral data and for providing the Spectral Visualization Toolkit. This work was part of the PERICLES project funded by the UK NERC. Data were obtained from the US DOE ARM Program.

[22] The Editor thanks two anonymous reviewers for their assistance in evaluating this paper.

References

Atlas, D., R. C. Srivastava, and R. S. Sekhon (1973), Doppler radar characteristics of precipitation at vertical incidence, *Rev. Geophys.*, *11*, 1–35.

Doviak, R. J., and D. S. Zrnić (1984), *Doppler Radar and Weather Observations*, Academic Press, New York.

Ellis, S. M., and J. Vivekanandan (2011), Liquid water content estimates using simultaneous S and K_a band radar measurements, *Radio Sci.*, *46*, RS2021, doi:10.1029/2010RS004361.

Gaussiat, N., H. Sauvageot, and A. J. Illingworth (2003), Cloud liquid water and ice content retrieval by multiwavelength radar, *J. Atmos. Oceanic Technol.*, *20*, 1264–1275.

Hildebrand, P. H., and R. S. Sekhon (1974), Objective determination of the noise level in Doppler spectra, *J. Appl. Meteorol.*, *13*, 808–811.

Hogan, R. J., N. Gaussiat, and A. J. Illingworth (2005), Stratocumulus liquid water content from dual-wavelength radar, *J. Atmos. Oceanic Technol.*, *22*, 1207–1218.

Kollias, P., B. Albrecht, and F. Marks (2002), Why Mie? Accurate observations of vertical air velocities and raindrops using a cloud radar, *Bull. Am. Meteorol. Soc.*, *83*, 1471–1483.

Kollias, P., E. E. Clothiaux, M. A. Miller, B. A. Albrecht, G. L. Stephens, and T. P. Ackerman (2007), Millimeter-wavelength radars: New frontier in atmospheric cloud and precipitation research, *Bull. Am. Meteorol. Soc.*, *88*, 1608–1624.

Kollias, P., J. Rémillard, E. Luke, and W. Szyrmer (2011), Cloud radar Doppler spectra in drizzling stratiform clouds: 1. Forward modeling and remote sensing applications, *J. Geophys. Res.*, *116*, D13201, doi:10.1029/2010JD015237.

Liao, L. A., and R. Meneghini (2011), A study on the feasibility of dual-wavelength radar for identification of hydrometeor phases, *J. Appl. Meteorol. Climatol.*, *50*, 449–456.

Mather, J. H., and J. W. Voyles (2013), The ARM climate research facility: A review of structure and capabilities, *Bull. Am. Meteorol. Soc.*, *94*, 377–392.

Matrosov, S. Y. (1998), A dual-wavelength radar method to measure snowfall rate, *J. Appl. Meteorol.*, *37*, 1510–1521.

Meneghini, R., L. Liao, S. Tanelli, and S. L. Durden (2012), Assessment of the performance of a dual-frequency surface reference technique over ocean, *IEEE Trans. Geosci. Remote Sens.*, *50*, 2968–2977.

Piironen, P., and E. W. Eloranta (1994), Demonstration of a high-spectral-resolution lidar based on an iodine absorption filter, *Opt. Lett.*, *19*, 234–236.

Tridon, F., A. Battaglia, P. Kollias, E. Luke, and C. R. Williams (2013), Signal postprocessing and reflectivity calibration of the Atmospheric Radiation Measurement Program 915-MHz wind profilers, *J. Atmos. Oceanic Technol.*, *30*, 1038–1054.

Wang, Z., G. M. Heymsfield, L. Li, and A. J. Heymsfield (2005), Retrieving optically thick ice cloud microphysical properties by using airborne dual-wavelength radar measurements, *J. Geophys. Res.*, *110*, D19201, doi:10.1029/2005JD005969.